TOXICOLOGICAL SCIENCES **127(2)**, 474–484 (2012)
doi:10.1093/toxsci/kfs119
Advance Access publication March 29, 2012

Hepatic and Pulmonary Toxicogenomic Profiles in Mice Intratracheally Instilled With Carbon Black Nanoparticles Reveal Pulmonary Inflammation, Acute Phase Response, and Alterations in Lipid Homeostasis

Julie A. Bourdon,* Sabina Halappanavar,* Anne T. Saber,† Nicklas R. Jacobsen,† Andrew Williams,* Håkan Wallin,† Ulla Vogel,† and Carole L. Yauk*,[1]

*Environmental Health Sciences and Research Bureau, Mechanistic Studies Division, Health Canada, Ottawa, Canada, K1A 0K9; and †National Research Centre for the Working Environment, Copenhagen DK-2100, Denmark

[1]To whom correspondence should be addressed at Health Canada, Environmental Health Sciences and Research Bureau, Mechanistic Studies, 50 Colombine Drive, Tunney's Pasture, Ottawa, ON K1A 0K9, Canada. Fax: (613) 941-8530. E-mail: carole.yauk@hc-sc.gc.ca.

Received January 26, 2012; accepted March 14, 2012

Global pulmonary and hepatic messenger RNA profiles in adult female C57BL/6 mice intratracheally instilled with carbon black nanoparticles (NPs) (Printex 90) were analyzed to identify biological perturbations underlying systemic responses to NP exposure. Tissue gene expression changes were profiled 1, 3, and 28 days following exposure to 0.018, 0.054, and 0.162 mg Printex 90 alongside controls. Pulmonary response was marked by increased expression of inflammatory markers and acute phase response (APR) genes that persisted to day 28 at the highest exposure dose. Genes in the 3-hydroxy-3-methylglutaryl-Coenzyme A (HMG-CoA) reductase pathway were increased, and those involved in cholesterol efflux were decreased at least at the highest dose on days 1 and 3. Hepatic responses mainly consisted of the HMG-CoA reductase pathway on days 1 (high dose) and 28 (all doses). Protein analysis in tissues and plasma of 0.162 mg Printex 90–exposed mice relative to control revealed an increase in plasma serum amyloid A on days 1 and 28 ($p < 0.05$), decreases in plasma high-density lipoprotein on days 3 and 28, an increase in plasma low-density lipoprotein on day 28 ($p < 0.05$), and marginal increases in total hepatic cholesterol on day 28 ($p = 0.06$). The observed changes are linked to APR. Although further research is needed to establish links between observations and the onset and progression of systemic disorders, the present study demonstrates the ability of NPs to induce systemic effects.

Key Words: **systems biology; nanotoxicology; DNA microarrays.**

There is a growing number of commercial products containing nanoparticles (NPs, defined as particles between 1 and 100 nm in at least one dimension), which could lead to increased occupational exposures. NPs vary significantly in their size, surface area, shape, composition, charge, and surface chemistry compared with their bulk counterparts. Studies suggest that NPs readily infiltrate deeper pulmonary regions, are capable of interacting with subcellular structures such as DNA, and are able to move readily across cellular and tissue barriers (Vishwakarma *et al*., 2010). Consequently, some NPs exhibit increased toxicity in comparison to larger particles. Upon inhalation, they have been associated with a variety of adverse biological and physiological responses including inflammation, fibrosis, genotoxicity, and carcinogenicity (Hubbs *et al*., 2011).

As inhalation is a primary route of exposure for most NPs, the pulmonary effects of various nanomaterials have been well documented. It has also been established that NPs can induce systemic effects in organs remote from the primary site of exposure. For example, mice and rats exposed to carbon-based NPs via inhalation or intratracheal instillation exhibit oxidative stress, cardiovascular effects, and genotoxicity in various tissues (Moller *et al*., 2010) including the systemic microvascular wall (Nurkiewicz *et al*., 2006) and liver (Jackson *et al*., 2012; Nurkiewicz *et al*., 2006). One suggested mechanism for such distal effects is the physical translocation of the NPs into systemic circulation. However, it is estimated that very limited amounts of deposited NPs translocate into circulation (Sadauskas *et al*., 2009), and systemic effects have been observed with negligible particle translocation (Jackson *et al*., 2012). These distal effects may result from NP-induced molecular signaling cascades in lung tissue, which in turn initiate downstream toxic responses in secondary organs. For example, pulmonary inflammation and oxidative stress following NP exposure may result in the release of cytokines, chemokines, and reactive oxygen species into systemic circulation. Furthermore, pulmonary exposure to NPs may activate receptors leading to imbalances in the autonomic nervous system and the development of cardiac arrhythmia, as suggested in epidemiological studies of humans exposed to fine

and ultrafine particles (Magari *et al*., 2001). Although the mechanisms by which NPs may induce systemic effects have been inferred, the biological processes and the underlying molecular pathways leading to such systemic toxicities remain unclear and warrant further investigation.

Carbon black NPs (CBNPs) are poorly soluble spherical particles of amorphous carbon. CBNPs, including Printex 90 (14 nm CBNP), are the dominating black pigment in printing inks, paints, and plastics, and large volumes are used as reinforcing agents in tires and other rubber goods. Concerns over CBNP safety arose in the mid 1990s, when it was demonstrated that chronic exposure of rats to carbon black had the potential to induce tumors similar to those observed with diesel exhaust particles (presumably via particle overload mechanisms) (Nikula *et al*., 1995). Occupational exposure to CBNPs is associated with decreased lung function (Gardiner *et al*., 2001), but it has not been conclusively demonstrated to be associated with lung cancer (International Agency for Research on Cancer, 2010). In animal models, chronic and subchronic exposure to poorly soluble NPs of low toxicity, including CBNPs, induce mutations (Driscoll *et al*., 1996) and lung tumors (Schins and Knaapen, 2007) that are most likely associated with inflammation and oxidative stress. Printex 90 CBNPs have been very well characterized and are used extensively as a reference material for toxicological evaluations of NPs. Thus, they are an ideal model for exploring systemic effects of NP exposure.

We recently demonstrated that exposure to Printex 90 induces sustained pulmonary inflammation and persistent genotoxicity in the lungs and livers of adult female mice (Bourdon *et al*., 2012). In the present study, we establish global pulmonary and hepatic messenger RNA transcriptional profiles using tissues from the same animals. In addition, we quantify plasma and tissue proteins to determine if exposure to Printex 90 initiates systemic signaling cascades potentially leading to effects in the liver. This study provides insight into the molecular events associated with systemic perturbations of cholesterol homeostasis that are likely associated with CBNP-induced adverse cardiovascular outcomes.

MATERIALS AND METHODS

Animal handling, exposure, and tissue collection. Animal handling, exposure and tissue collection have been described previously (Bourdon *et al*., 2012). Briefly, female C57BL/6 mice (Taconic, Denmark) were acquired at 5–6 weeks of age and given food (Altromin no 1324; Christian Petersen; Denmark) and water *ad libitum*. All procedure complied with EC Directive 86/609/EEC and Danish laws regulating experiments on animals (permit 2010/561-1179).

Mice were exposed to 0.018, 0.054, and 0.162 mg Printex 90 CBNPs alongside controls for each postexposure day (1, 3, and 28 days). These doses equal the pulmonary deposition after 1, 3, and 9 working days for a mouse at the occupational exposure limit of 3.5 mg/m^3 CB per 8 h work shift (as established by the Occupational Safety and Health Administration and the National Institute for Occupational Safety and Health). These calculations assume that 33.8% of the inhaled mass ends up in the pulmonary region with a volume of inhaled air per hour of 1.8 l/h and 8 h working days as described in Jacobsen *et al*. (2009). The mice did not display any signs of respiratory distress, decreased locomotor activity, lethargy, or any other physical symptoms of exposure.

Printex 90 was suspended by sonication in 0.9% NaCl MilliQ water containing 10% vol/vol acellular bronchial alveolar lavage fluid from C57BL/6 mice. A total of 72 mice (six per group) were given 0.018, 0.054, or 0.162 mg of Printex 90 CBNPs by single intratracheal instillation. Before the intratracheal instillation, the mice were anesthetized using Hypnorm (fentanyl citrate 0.315 mg/ml and fluanisone 10 mg/ml from Janssen Pharma) and Dormicum (midazolam 5 mg/ml from Roche).

The trachea of each mouse was intubated using a 24 gauge BD Incyte catheter (Becton Dickinson, Denmark) with a shortened needle. The proper location of the catheter was ensured using a highly sensitive pressure transducer developed at the National Research Centre for the Working Environment in collaboration with John Frederiksen (FFE/P, Denmark). A 40 µl suspension was instilled followed by 150 µl air with a 250 µl SGE glass syringe (250F-LT-GT; MicroLab, Aarhus, Denmark). Control animals received 40 µl vehicle instillations (0.9% NaCl MilliQ water containing 10% vol/vol acellular bronchoalveolar lavage [BAL] from C57BL/6 mice). Mice were placed on a 37°C heating pad to recover from anesthesia. One, 3, and 28 days after the instillation, the mice were anesthetized with Hypnorm/Dormicum as described above. Heart blood (800–1000 µl) was stabilized in 72 µl 0.17M K_2EDTA and kept on ice until plasma was isolated by centrifugation at 2000 × g for 10 min (4°C). BAL fluid, lung, and liver were collected immediately after withdrawing the heart blood. Tissues were frozen in liquid nitrogen and stored at −80°C.

Particle characterization. Printex 90 CBNPs were a gift from Evonik/Degussa (Frankfurt, Germany). The hydrodynamic particle size distributions in the exposure media were determined by dynamic light scattering (DLS) using a Malvern Zetasizer Nano ZS, as described previously (Bourdon *et al*., 2012). Agglomeration levels were also assessed by transmission electron microscopy. DLS analysis of the exposure media was performed on the raw instillation dispersions and after filtration through 3 µm (Glass Micro Fiber; Whatman, U.K.) and 0.2 µm (hydrophilic DISMIC-25CS Cellulose Acetate; Toyo Roshi Kaisha Ltd, Japan) syringe filters.

Total RNA extraction. Total RNA was isolated from lung and liver tissue of 72 mice in total ($n = 6$ mice per group). Isolations were done using TRIzol reagent (Invitrogen, Canada) and purified using the RNeasy MiniKit (Qiagen, Canada). An on-column DNase treatment was applied (Qiagen). RNA concentrations were determined using a NanoDrop 2000 spectrophotometer (Thermo Scientific, Canada). RNA quality was assessed using a BioAnalyzer (Agilent Technologies, Canada), and only RNA with RNA integrity numbers above 7.5 was used in the experiment. Total RNA was stored at −80°C until analysis.

Microarray hybridization. Total RNA (200 ng) from each sample ($n = 6$ per group), alongside Stratagene universal mouse reference RNA (Agilent, Canada), was used to synthesize double-stranded complementary DNA (cDNA) and cyanine-labeled complementary RNA (cRNA) using the Agilent Linear Amplification kit (Agilent Technologies). Experimental samples were labeled with cyanine 5-CTP, whereas reference RNA was labeled with cyanine 3-CTP (PerkinElmer Life Sciences, Canada). The cyanine-labeled cRNA was *in vitro* transcribed using T7 polymerase and purified using RNeasy mini kits (Qiagen). Sample and reference targets (825 ng) were combined and hybridized to Agilent 4 x 44K oligonucleotide microarrays (Agilent Technologies) for 17 h at 60°C. The arrays were washed according to supplier instructions and then scanned on an Agilent G2505B scanner at 5 µm resolution. Data were acquired using Agilent Feature Extraction software version 9.5.3.1.

Statistical analysis of microarray data. A reference design was employed to determine global differential gene expression, and randomized blocks were used to offset interarray effects. Median signal intensities were normalized using LOWESS in R, and differential gene expression was determined using the microarray analysis of variance (MAANOVA) library (R Development

Core Team, 2010). The *Fs* statistic, a shrinkage estimator, was used to determine gene-specific treatment effects, and the associated *p* values were estimated using the permutation method (30,000 permutations with residual shuffling). Data were adjusted for multiple comparisons using the Benjamini and Hochberg false discovery rate (FDR) approach to limit false-positive results. Fold changes were based on least square means of each pairwise comparison. *p* values and fold changes for probes of the same target were averaged. Genes having an FDR-adjusted $p < 0.1$ and a fold change > 1.5 were deemed differentially expressed.

Data quality was evaluated in GeneSpring GX version 11.5.1 (Agilent Technologies). Dye bias was determined by generating MA plots and scatter plots. Outliers were identified using hierarchal clustering and box plots. Mining of the pathways and processes represented among the significant genes was conducted in Ingenuity Pathway Analysis version 8.6. A right-tailed Fisher's exact test was used to calculate *p* values for each biological pathway. DAVID Bioinformatics Resources 6.7 was used to identify enriched biological functions from terms with similar genes and biological meaning (Huang *et al*., 2009a,b). Biological functions with enrichment scores > 1.3 were considered significant, in accordance with DAVID recommendations (Huang *et al*., 2009b).

Real-time PCR. Primers were designed within the same exon as the Agilent microarray probe sequence using Beacon Designer 2.0 (Premier BioSoft International, USA). Primer specificity was assured by melting curve analysis, and optimal annealing temperatures were determined by gradient PCR experiments. Total RNA (1 μg) from lung and liver was reverse transcribed to cDNA for each sample ($n = 4$ per group), using the SuperScript III First-Strand Synthesis system (Invitrogen). Real-time quantitative PCR was performed on 10-fold cDNA dilutions in duplicate using a CFX96 real-time PCR detection system (Bio-Rad, Canada). Threshold cycle values were averaged. PCR efficiency for both the gene of interest and the reference gene was extrapolated from a standard curve, established by a fivefold serial dilution of pooled cDNA. Fold changes were calculated according to the $2^{-\triangle\triangle CT}$ method, using the CFX manager software (Bio-Rad). Statistical inference was established using the REST program version 2.0.13 (Pfaffl *et al*., 2002).

PCR arrays. PCR arrays were employed for analysis of transcripts involved in inflammatory responses, oxidative stress, and cholesterol efflux in lung. The complete list of genes and the results obtained for PCR arrays can be found in Supplementary table 3. Total RNA (1 μg) from lung was reverse transcribed into cDNA using an RT^2 First Strand Kit (SABiosciences, USA). RT^2 SYBR Green PCR master mix was employed for real-time PCR, and experiments were carried out using a CFX96 real-time PCR detection system (Bio-Rad). Threshold cycles were averaged.

Using the delta CT values, differentially expressed genes were identified using a two-sample bootstrap test (t-pivot method) assuming unequal variances using the R software (Higgins, 2003). Standard errors for the fold change for each comparison were estimated using the bootstrap method.

Total lipid extraction and total hepatic cholesterol analysis. Total lipids were extracted from liver tissue according to the Folch method. Briefly, liver tissue was homogenized in 500 μl equal volumes of methanol and water. A double volume of 5:1 chloroform/methanol was then added, and phases were separated by centrifugation. The lower chloroform lipid–containing layer was separated, and chloroform removed under nitrogen gas flow. Lipids were resuspended in 100 μl EnzyChrom assay buffer and stored at −20°C until analysis.

The EnzyChrom AF Cholesterol Assay Kit (BioAssay Systems, USA) was employed for quantitative colorimetric determination of hepatic cholesterol levels ($n = 6$ per group; 0.162 mg dose group and controls), according to manufacturer recommendations. Briefly, lipid extracts from each sample and a serial dilution of a standard cholesterol reference supplied by the manufacturer were diluted 10-fold, and 50 μl aliquots were placed in a clear 96-well plate, in duplicate. Fifty microliter of a dye reagent-enzyme mix was added, and the plate was incubated at room temperature for 30 min. The color intensity of the reaction product was spectrophotometrically measured at 570 nm, and total cholesterol concentrations were determined by comparison to the standard curve, with normalization to extracted tissue weight. Statistical significance was determined using an unpaired one-tailed *t*-test assuming unequal variances.

Plasma high-density lipoprotein, low-density lipoprotein/very low-density lipoprotein, and total cholesterol analysis. Fluorimetric quantification of cholesterol was determined in plasma using the EnzyChrom AF HDL and LDL/VLDL assay kit (BioAssay Systems) according to the manufacturer's instructions ($n = 6$ per group; 0.162 mg dose group and controls). HDL isolation was performed by collection of the supernatant following centrifugation of a 1:1 plasma-precipitating reagent solution. The low-density lipoprotein/very low-density lipoprotein (LDL/VLDL) fraction was separated by dissolution of the collected pellet in PBS. Plasma, high-density lipoprotein (HDL), and LDL/VLDL isolations from each sample and a serial dilution of a standard cholesterol reference supplied by the manufacturer were diluted 10-fold, and 50 μl aliquots were placed in a clear 96-well plate, in duplicate. Fifty microliter of a dye reagent-enzyme mix was added, and the plate was incubated at room temperature for 30 min. Fluorescence measurements were recorded on a SpectraMax M2 (Molecular Devices, USA) at 530 nm (excitation) and 585 nm (emission), and cholesterol concentrations were determined by comparison to a standard curve. Statistical inference was determined using an unpaired one-tailed *t*-test assuming unequal variances.

Plasma serum amyloid A analysis. Total serum amyloid A (SAA) was measured in plasma samples using the PhaseRange Mouse SAA ELISA kit (Tridelta Development Ltd, Ireland), according to manufacturer's instructions ($n = 6$ per group; 0.162 mg dose group and controls). Briefly, plasma from each mouse and a serial dilution of a standard SAA reference supplied by the manufacturer were diluted 200-fold and mixed with an equal volume of anti-SAA horseradish peroxidase (HRP) conjugate. One hundred microliter of each plasma-antibody solution was loaded in duplicate in a 96-well plate precoated with SAA antibody, incubated for 1 h at 37°C and subjected to four wash cycles. A streptavidin-HRP enzyme was then added to each well and incubated for 15 min at room temperature. The reaction was quenched by the addition of 100 μl of stop solution. Absorbance measurements were read at 450 nm with a SpectraMax M2 (Molecular Devices, USA), and SAA concentrations were determined by comparison to the standard curve. Statistical inference was determined by unpaired one-tailed *t*-test, assuming unequal variances.

RESULTS

Particle Characterization

Printex 90 CBNPs have been characterized extensively in Bourdon *et al.* (2012). A summary of this particle characterization can be found in Table 1. Briefly, the manufacturer declares a primary particle size of 14 nm. The reported polycyclic aromatic hydrocarbon and endotoxin content reported in Table 1 are not expected to cause biological effects, as described thoroughly in Bourdon *et al.* (2012); Jacobsen *et al.* (2007, 2008). CBNPs within instillation vehicle displayed a high degree of agglomeration, which is in accordance with the low zeta potential reported. DLS analysis of the raw instillation vehicle revealed that the suspension was highly polydisperse, with a peak size of approximately 2.6 μm. Size distribution of these agglomerates was broad, ranging from less than 100 nm but typically 200 nm or larger. The largest of the agglomerates were in the range of 20–30 μm.

TABLE 1
Physical-Chemical Properties of Printex 90 as a Raw Material and in Vehicle (0.9% NaCl MilliQ Water Containing 10% vol/vol Acellular BAL)

Particle characterization	
Manufacturer declared size (nm)	14
Surface area (BET) (m^2/g)	295–338
Pycnometric particle density (g/cm^3)	2.1
Chemical composition	99% C, 0.8% N, and 0.01% H_2
Polycyclic aromatic hydrocarbon (ng/g)	74.2
Endotoxin (EU/g)	142
Particle properties in vehicle	
Polydispersity index	1
Zeta potential (mV)	−10.7
Peak hydrodynamic number (μm)	2.6
Peak volume-size distribution (μm)	3.1
Morphology	Free and open chain aggregates with minor amounts of free single primary spheres

This wide distribution is in agreement with the very elevated polydispersity index observed. Filtering (3.1 and 0.2 μm) of the raw dispersion vehicle revealed the presence of smaller particles.

Inflammatory Cell Influx in BAL

The animals used in this study were from a previous experiment. Details of this study can be found in Bourdon *et al.* (2012). Briefly, characterization of the cell composition of BAL revealed elevated total BAL cell counts 1 and 3 days postexposure for all doses (0.018, 0.054, and 0.162 mg) and sustained increases for the medium and high doses up to the 28-day time point. This response was primarily dominated by increases in neutrophils at all doses and time points studied. Eosinophils and lymphocytes were also increased at all doses but only at the 3-day time point. BAL cell counts for neutrophils, eosinophils, macrophages, lymphocytes, and total BAL cells are presented in Supplementary figures 1A–E.

Global Pulmonary Differential Gene Expression

Gene expression microarray analysis was conducted on the left lung lobe (whole tissue) from a total of 72 mice ($n = 6$ per treatment group) exposed to vehicle (control), 0.018, 0.054, and 0.162 mg of Printex 90 CBNPs by a single intratracheal instillation and necropsied 1, 3, and 28 days postexposure. MA plots, box plots, and cluster analyses of normalized signal intensities for all probes revealed that 5 of 72 microarrays produced substandard data quality (data not shown). These arrays were distributed across treatment conditions and were removed from the analysis. The MAANOVA analysis was thus conducted on a final sample size of at least five mice per treatment group to identify differentially expressed genes. Genes with FDR-adjusted $p < 0.1$ and fold changes > 1.5 in either direction were considered differentially expressed.

MAANOVA analysis revealed that 487 genes were significantly differentially expressed (upregulated or downregulated relative to control samples) in at least one of the treatment conditions. The complete list is presented in Supplementary table 1A. There were 2, 45, and 294 differentially expressed genes 1 day postexposure and 0, 11, and 201 differentially expressed genes 3 days postexposure in the 0.018, 0.054, and 0.162 mg dose groups, respectively. At 28 days postexposure, the high-dose group showed 123 altered genes, but no effects were observed for the two lower doses. Thus, the low-dose treatment groups had very little effect on the global expression profiles as measured on DNA microarrays. The number of genes that were in common between the 0.162 mg dose across time points is shown in a Venn diagram in Supplementary figure 2A. Cluster analysis revealed dose-response trends within time points with similar pathways/functions affected at the high dose and the lower doses. The results demonstrate substantial changes over time in the subset of genes differentially affected by the Printex 90 exposure (evident within the 0.054 and 0.162 mg doses only as shown by heat maps in Supplementary figs. 2B and C). The complete microarray dataset is available through the Gene Expression Omnibus at NCBI (http://www.ncbi.nlm.nih.gov/geo/, Superseries GSE35284, SubSeries GSE35193).

Data mining using DAVID functional annotation clustering to determine functional groups of similar genes and affected biological processes revealed 40 annotations with enrichment scores > 1.3 (Supplementary table 2A). These biological functions were mostly related to inflammatory, immune, and acute phase responses (APRs) but also included changes in sterol biosynthesis, apoptosis signaling, and cell cycle regulation. Ingenuity pathway analysis of the high-dose group revealed the predominance of inflammatory and immune responses across all time points (Supplementary fig. 2D). Transcript changes for genes involved in inflammation (29 genes), cholesterol transport (2 genes), oxidative stress, and antioxidant responses (8 genes) were validated using PCR arrays and showed a high correlation with the DNA microarray results (Supplementary table 3A).

Global Hepatic Differential Gene Expression

Because major persistent effects were only observed in the lungs at the highest doses, hepatic microarray gene expression profiling was only conducted on mice exposed to 0.162 mg CBNPs and sacrificed 1, 3, and 28 days postexposure. Six outliers were removed from the analysis based on quality control metrics (MA plots, box plots, and cluster analysis of normalized signal intensities for reference RNA and biological samples). MAANOVA analysis was conducted on a final sample number of at least four per treatment group to identify differentially expressed genes. Genes with FDR-adjusted

TABLE 2
Expression Over Control of Acute Phase Response Signaling Genes Measured by Agilent 4 x 44K Microarray Analysis in C57BL/6 Mice Exposed to 0.162 Printex 90 CBNPs and Sacrificed 1, 3, and 28 Days Postexposure. Fold Changes Over Matched Controls and *p* Value Are Presented

	Day 1		Day 3		Day 28	
Gene name	Fold change	*p* Value	Fold change	*p* Value	Fold change	*p* Value
Lung						
Serum amyloid A3 (*Saa3*)	**65.3**	**0.00**	**8.3**	**0.00**	6.8	0.00
Metallothionein 2 (Mt2)	**5.7**	**0.00**	**2.1**	**0.00**	1.3	0.30
Ceruloplasmin (*Cp*)	**3.5**	**0.00**	**2.2**	**0.00**	1.1	0.55
Metallothionein 1 (*Mt1*)	**2.1**	**0.00**	**1.7**	**0.00**	1.2	0.06
Serum amyloid A1 (*Saa1*)	**11.3**	**0.00**	1.7	0.02	1.5	0.07
Serum amyloid A2 (*Saa2*)	**6.9**	**0.00**	1.4	0.11	1.3	0.23
Orosomucoid 2 (*Orm2*)	**3.6**	**0.00**	1.3	0.19	1.4	0.12
Orosomucoid 1 (*Orm1*)	**2.6**	**0.00**	1.1	0.42	1.2	0.15
Complement component 3 (*C3*)	**2.0**	**0.00**	1.4	0.00	1.5	0.01
Liver						
Serum amyloid A3 (*Saa3*)	**4.2**	**0.00**	1.0	0.91	0.5	0.96
Orosomucoid 3 (*Orm3*)	2.2	0.02	0.5	0.98	1.0	0.92
Serum amyloid A1 (*Saa1*)	1.5	0.03	0.6	0.77	0.6	0.27
C-reactive protein (*Crp*)	1.0	0.92	1.5	0.10	1.7	0.03

Note. Data in bold are FDR significant (< 0.1).

p value < 0.1 and fold changes > 1.5 in either direction were considered significant (differentially expressed) and were analyzed in detail. The analysis revealed 81 differentially expressed genes (upregulated and downregulated) overall (Supplementary table 1B). Within time points, 53, 2, and 26 changes in transcripts were found on days 1, 3, and 28, respectively. None of the genes identified overlapped across time points as shown in the Venn diagram in Supplementary figure 1E. Cluster analysis revealed clear exposure effects on day 1 and day 28 but not on day 3 as shown in the heat map in Supplementary figure 2F. Microarray data are available through the Gene Expression Omnibus at NCBI (http://www.ncbi.nlm.nih.gov/geo/, SuperSeries GSE35284, SubSeries 35192).

DAVID functional annotation clustering revealed four biological functions with an enrichment score > 1.3 (Supplementary table 2B). These clusters were related to sterol and terpenoid biosynthesis, cytochrome p450 and cell movement. Ingenuity pathway analysis of biological functions across time points also revealed lipid metabolism as the primary process perturbed in liver by Printex 90 exposure (Supplementary fig. 2G).

Inflammation and APR Signaling in Lung, Liver, and Plasma

Mining of lung microarray data by Ingenuity pathway analysis showed that approximately 38% of the differentially expressed genes were directly associated with inflammatory responses. In the high-dose groups, upregulated expression of several of these genes, including chemokine (C-C motif) ligands 2 (*Ccl2*), *Ccl3*, *Ccl8*, *Ccl9*, and *Ccl12* was evident on day 1 and persisted up to 28 days postexposure, with fold changes ranging from 1.5- to 5.0-fold above control animals. Twenty-nine genes involved in inflammation were validated using PCR arrays and correlated highly with the DNA microarray results (Supplementary table 3A).

The highest fold changes in the lungs of mice intratracheally instilled with CBNPs were attributed to SAA genes (*Saa1*, *Saa2*, and *Saa3*) and other genes involved in APR signaling, including metallothioneins and orosomucoids (Table 2). Quantitative real-time PCR analysis in lung revealed that *Saa1* and *Saa3* were also affected at lower doses of exposure (i.e., all doses on postexposure day 3) and at later time points (i.e., the 0.162 mg dose on postexposure day 28) (Supplementary table 3B). Our results correlate strongly with previous measurements of *Saa3* in the same tissue (Bourdon *et al.*, 2012). However, we could not validate the upregulation of *Saa3* in liver by quantitative real-time PCR (Bourdon *et al.*, 2012).

To confirm the presence of SAA protein, we measured total SAA levels in plasma of an additional set of mice exposed to 0.162 mg CBNPs using identical exposure procedures. Total SAA levels were increased by 15.3% on postexposure day 1 (from 1.2 to 1.4 mg/dl; $p < 0.05$), by 15.6% on day 3 (from 1.1 to 1.3 mg/dl; $p = 0.0789$), and by 11.8% on day 28 (from 1.0 to 1.1 mg.dl; $p < 0.05$) (Fig. 1A).

Alterations in Cholesterol Homeostasis

Pulmonary and hepatic gene expression profiling in parallel with plasma analysis strongly suggested systemic alterations in

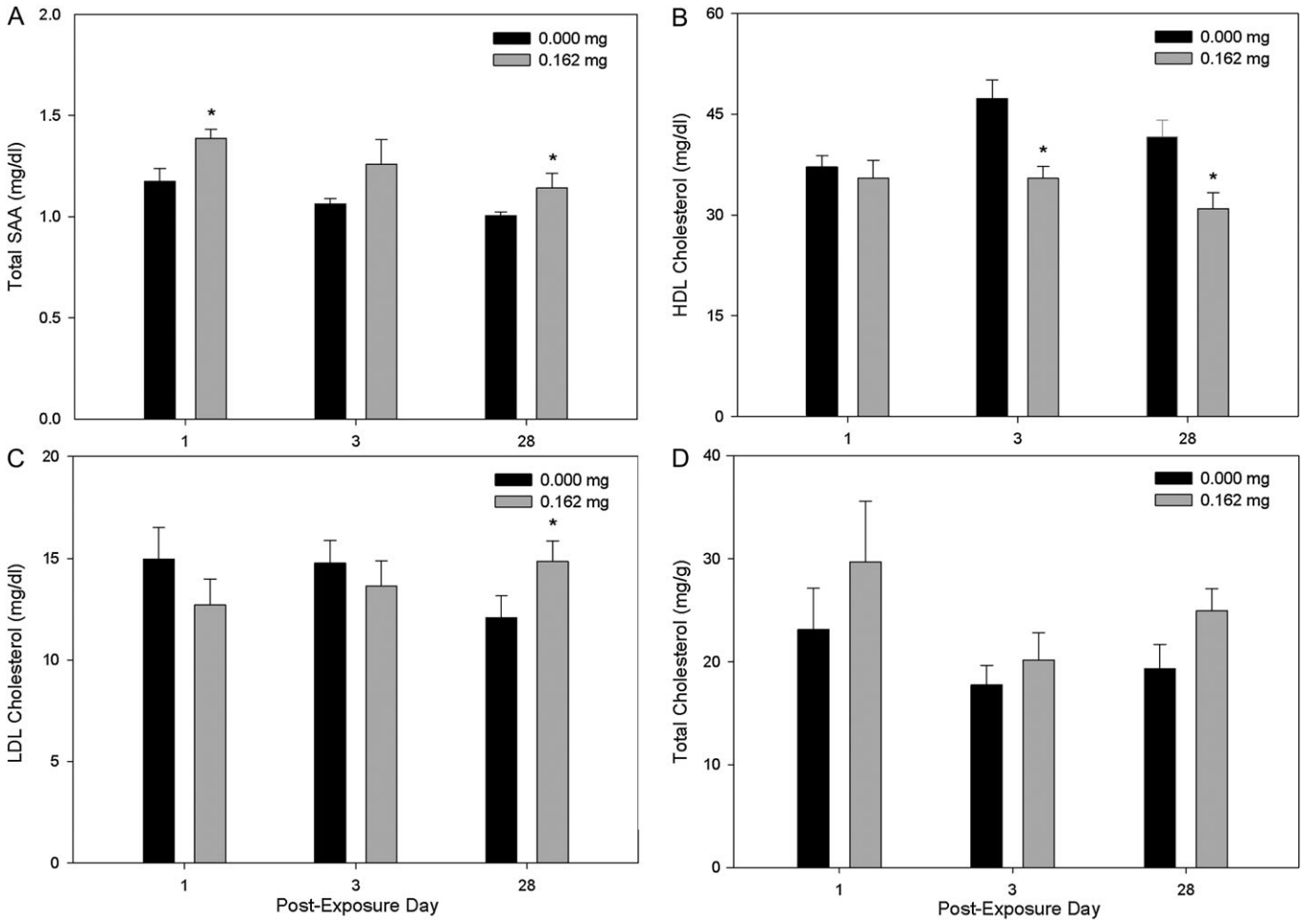

FIG. 1. Changes in (A) plasma total SAA, (B) plasma HDL, (C) plasma LDL, and (D) hepatic total cholesterol in C57BL/6 mice exposed to vehicle and 0.162 mg Printex 90 CBNPs and sacrificed 1, 3, and 28 days postexposure. Significance was calculated by comparison to matched control, and * indicates $p < 0.05$.

cholesterol homeostasis. Pulmonary gene expression profiles of the high-dose group revealed significant upregulation of genes involved in cholesterol synthesis, on postexposure days 1 and 3 relative to control mice (Table 3). DAVID functional annotation clustering revealed this subset of genes to be involved directly in sterol and terpenoid biosynthesis (enrichment score = 3.4) (Supplementary table 2A). These biological functions collectively form the 3-hydroxy-3-methylglutaryl-Coenzyme A (HMG-CoA) reductase pathway, which is the rate-limiting pathway of cholesterol synthesis. Two genes of this pathway (*Sqle* and *Fdps*) were confirmed by quantitative real-time PCR in lung (Supplementary table 3B).

Microarray analysis of pulmonary profiles also demonstrated substantial downregulation of cholesterol efflux gene ATP-binding cassette subfamily G member 1 (*Abcg1*, −1.7-fold) at the highest exposure dose on day 1. Quantitative real-time PCR of *Abcg1* and associated ATP-binding cassette subfamily A member 1 (*Abca1*) showed 2.3- and 2.6-fold downregulation of *Abcg1* and *Abca1* on day 1, and 1.8-fold downregulation of *Abcg1* on day 3 (Supplementary table 3A).

Substantial upregulation of the HMG-CoA reductase pathway was also found in liver, as demonstrated by the highly enriched sterol and terpenoid biosynthesis cluster using DAVID functional annotation clustering (enrichment score = 7.7) (Supplementary table 2B). The pathway was perturbed on postexposure day 1 in the high-dose mice, relative to controls. Expression changes were fairly consistent across these genes, ranging from a 1.6- to a 2.6-fold increase in treated over control mice (Table 3). In order to clarify whether the HMG-CoA reductase pathway activity is also affected at later time points and lower doses of exposure, we measured *Hmgcr*, *Dhcr7*, *Fdps*, *Mvd*, and *Sqle* transcript levels using quantitative real-time PCR. Our microarray findings were confirmed for postexposure day 1. However, many genes were also found to be differentially expressed on day 28 at all exposure doses (Supplementary table 3B).

In order to substantiate changes in cholesterol synthesis, we measured cholesterol levels in plasma and livers of the mice. Plasma analysis in the additional mice exposed according to the same exposure regimen (high dose and controls only) revealed

TABLE 3
Expression of Genes Part of the HMG-CoA Reductase Pathway Measured by Agilent 4 x 44K Microarray Analysis in C57BL/6 Mice Exposed to 0.162 Printex 90 CBNPs and Sacrificed 1, 3, and 28 Days Postexposure. Fold Changes Over Matched Controls and *p* Value Are Presented

	Day 1		Day 3		Day 28	
Gene name	Fold change	*p* Value	Fold change	*p* Value	Fold change	*p* Value
Lung						
Squalene epoxidase (*Sqle*)	**1.6**	**0.00**	**1.8**	**0.00**	1.2	0.04
Isopentyl-diphosphate delta isomerase (*Idi*)	**1.4**	**0.00**	**1.7**	**0.00**	1.2	0.11
Farnesyl-diphosphate synthase (*Fdps*)	1.3	0.02	**1.6**	**0.00**	1.3	0.02
Diphosphomevalonate decarboxylase (*Mvd*)	1.4	0.01	**1.5**	**0.00**	1.3	0.03
Liver						
3-Hydroxy-3-methylglutaryl-CoA reductase (*Hmgcr*)	**2.8**	**0.00**	0.5	0.67	2.4	0.00
Lanosterol synthase (*Lss*)	**2.6**	**0.00**	1.2	0.34	1.3	0.08
Isopentyl-diphosphate delta isomerase (*Idi*)	**2.3**	**0.00**	1.2	0.10	1.5	0.03
HMG-CoA synthase (*Hmgcs1*)	**2.0**	**0.00**	1.2	0.28	1.4	0.13
Squalene epoxidase (*Sqle*)	**1.9**	**0.00**	1.2	0.33	1.2	0.25
Mevalonate kinase (*Mvk*)	**1.9**	**0.00**	1.2	0.12	1.2	0.12
Farnesyl-diphosphate synthase (*Fdps*)	**1.8**	**0.00**	1.1	0.30	1.2	0.08
7-Dehydrocholesterol reductase (*Dhcr7*)	**1.6**	**0.00**	1.1	0.48	1.2	0.24
Diphosphomevalonate decarboxylase (*Mvd*)	1.9	0.00	0.5	0.79	1.1	0.98

Note. Data in bold are FDR significant (< 0.1).

no effects of CBNP exposure on total plasma cholesterol (data not shown). However, HDL levels were decreased on postexposure days 3 and 28 ($p < 0.05$) by 21.8 and 25.7% (Fig. 1B). LDL levels were also increased by 18.8% on postexposure day 28 (Fig. 1C). Total cholesterol levels in hepatic tissues were marginally elevated in the 0.162 mg exposed mice groups on day 28 ($p = 0.06$) compared with sham controls. Overall, total hepatic cholesterol was increased by 22.2, 12.1, and 22.6% in the high-dose group on days 1, 3, and 28, respectively (Fig. 1D). We note that our cholesterol analyses resulted in some variability between postexposure day controls. The reason for this effect is unknown but may be related to the intratracheal instillation procedure.

DISCUSSION

We investigated pulmonary and hepatic gene expression in mice instilled with vehicle, 0.018, 0.054, and 0.162 mg Printex 90 CBNPs and sacrificed 1, 3, and 28 days after this single exposure. Gene expression profiles in lungs revealed large-scale CBNP-induced perturbations of inflammatory cytokine and chemokine transcripts, supported by concomitant changes in BAL cell counts. Large changes in acute phase SAA transcripts (*Saa1*, *Saa2*, and *Saa3*) were measured in the lungs up to 28 days postexposure for the highest dose group and up to 3 days postexposure in the lower dose groups relative to controls. Elevated SAA protein was confirmed in the plasma of mice exposed to 0.162 mg Printex 90 on postexposure days 1 and 28. Genes in the HMG-CoA reductase pathway were perturbed in both lung and liver. In the lung, these changes were observed at the two higher doses on postexposure days 1 and 3, whereas more substantial changes in liver were detected on days 1 (0.162 mg dose) and 28 (all doses). In parallel, HDL cholesterol was decreased relative to controls 3 and 28 days postexposure, whereas LDL cholesterol was increased at 28 days (i.e., 0.162 mg dose group). Thus, our genomic profiling demonstrates the cascade of events initiated through inflammation and APR in the lungs leading to liver transcriptional changes and impacting lipid homeostasis following NP exposure.

Inhalation of CBNPs can cause direct pulmonary injury, thus instigating an inflammatory response. Indeed, the inflammatory response was the overwhelming biological effect observed in our transcript profiles, supporting the observed phenotype. The proinflammatory genes identified were primarily involved in recruitment and activation of various inflammatory markers including neutrophils (*Cxcl5*, *Ccl3*, and *Cxcl1*), eosinophils, (*Ccl11*, *Ccl12*, and *Ccl8*), monocytes (*Ccl7*, *Ccl2*, *Ccl4*, *Cc12*, and *Ccl8*), and lymphocytes (*Ccl20*, *Ccl24*, and *Ccl12*) with large persisting increases in *Cxcl5* that may explain the predominance of neutrophils in our BAL cell profiles (Bourdon *et al*., 2012).

Inflammatory signaling molecules, including interleukin-6 and tumor necrosis factor (both upregulated by CBNP exposure), have been suggested to trigger the APR. APR is characterized by rapid induction of positive acute phase proteins (e.g., c-reactive protein, SAA, and serum amyloid P), decreases in negative acute phase proteins (e.g., albumin and transferrin), and physiological changes (e.g., altered metabolism

and fever). Generally, the APR is a transient response initiated to prevent further injury and to activate repair processes. Prolonged APR is linked to aortic inflammation and accelerated atherosclerosis, as observed in individuals with chronic inflammatory diseases including rheumatoid arthritis and systemic lupus erythematosus (Hollan *et al.*, 2007). It has also been shown that increased levels of SAA in plasma directly accelerate progression of atherosclerosis in $ApoE^{-/-}$ mice (Dong *et al.*, 2011). For such reasons, positive acute phase proteins (e.g., c-reactive protein, phospholipase A2, and SAA) are proposed biomarkers of potential cardiovascular disease (Ballantyne *et al.*, 2004). Inhalation of nano-sized nickel and titanium dioxide has been shown to initiate an APR in mouse (Halappanavar *et al.*, 2011; Kang *et al.*, 2011). Here, we demonstrate that a single installation of relatively low doses of CBNPs induces inflammation with an associated APR that can persist for 28 days. As such, we speculate that exposure to CBNPs and possibly other nanoparticulates may be associated with chronic inflammation-mediated APR, which in turn may increase susceptibility to cardiovascular disease.

One of the mechanisms by which inflammation-triggered APR may elicit adverse cardiovascular outcomes is through interruption of cholesterol transport (Feingold and Grunfeld, 2010). APR is implicated in disrupting reverse cholesterol transport at many levels, including reduced levels and altered functions of HDL, as well as reduced efficacy of cholesterol efflux and bile acid synthesis. HDL, which facilitates reverse cholesterol transport and inhibits the oxidation of LDL in healthy individuals, is greatly reduced in humans (Annema *et al.*, 2010) and in mice (McGillicuddy *et al.*, 2009) during the APR and in our study. Increased plasma levels of SAA observed in our study may lead to interruption of reverse cholesterol transport by displacement of apolipoproteins and replacement of cholesterol esters and phospholipids by triglycerides, unesterified cholesterol, and ceramides (Feingold and Grunfeld, 2010). Such modifications in HDL are suggested to inhibit both cholesterol efflux from macrophages and protection against LDL oxidation (Annema *et al.*, 2010; Feingold and Grunfeld, 2010; McGillicuddy *et al.*, 2009). These alterations may even allow HDL to participate in inflammatory responses and to deliver cholesterol to macrophages (Feingold and Grunfeld, 2010). In addition, APR also affects lipid transport by downregulating cholesterol efflux genes in peripheral tissues and by reducing hepatic cholesterol uptake and synthesis of bile acids (McGillicuddy *et al.*, 2009). Although we did not detect any alterations in hepatic cholesterol uptake or bile synthesis, we observed downregulation of cholesterol efflux genes *Abca1* and *Abcg1* in pulmonary tissue. Our results suggest that a single instillation of Printex 90 leads to inflammation and APR, which markedly alters systemic cholesterol transport and metabolism over a prolonged time scale. These processes can lead to adverse health outcomes when induced chronically.

Alterations in lipid transport (such as those described above) can trigger sterol-sensitive pathways in extra-pulmonary tissues. As a central site of metabolism, the liver plays an important role in regulating lipid homeostasis. The mice in the present study exhibited significant changes in hepatic expression of *Hmgcr*, which is rate limiting in the HMG-CoA reductase pathway and in *de novo* cholesterol production. HMG-CoA is exclusively activated under low-sterol conditions in a negative feedback loop and fulfills two important biological functions: (1) production of terpenoid intermediates to serve in the prenylation of small GTPases (e.g., Ras, Rac, and Rho) and activation of a variety of cellular processes (e.g., actin cytoskeleton remodeling, cellular proliferation, generation of reactive oxygen species, and inflammatory responses) (Liao, 2002) and (2) cholesterol production. Exposure to CBNP in the present study caused a fairly uniform upregulation of genes across this entire pathway (*Hmgcr*, *Mvd*, *Fdps*, *Sqle*, and *Dhcr7*). Upregulation of genes downstream of *Sqle* suggests that CBNP exposure tips this pathway toward cholesterol production. Cholesterol is critical for maintaining cellular membrane integrity (e.g., lipid rafts, signal transduction, and molecular exchanges). It has been established that severe inflammation, infection, and APR activate the HMG-CoA reductase pathway in the liver of rodents, as demonstrated in models of lipopolysaccharide treatment (Feingold *et al.*, 1993, 1995; Memon *et al.*, 1993). Here, we demonstrate that Printex 90 intratracheal instillation leads to upregulation of the HMG-CoA reductase pathway in liver and lung, with concomitant "modest" changes in plasma LDL and marginal increases in hepatic cholesterol. The results suggest that pulmonary CBNP responses trigger molecular signaling cascades affecting the liver, and that these responses may drive excess production of cholesterol. It is possible that perturbations of cholesterol homeostasis observed in our work may be further exacerbated by the protein corona created around CBNPs. A recent study using N-isopropylacrylamide and N-t-butylacrylamide copolymers of varying size and composition demonstrates that NPs bind cholesterol, triglycerides, and phospholipids (with preference to HDL) and that binding reaches saturation (Hellstrand *et al.*, 2009). This effect is strongest with increased hydrophobicity and surface area of the particle and thus relevant to the chemical properties of Printex 90 CBNPs. Therefore, this may be an additional mechanism by which the HMG-CoA reductase pathway is upregulated in the present study.

Exposure to fine and ultrafine particles is associated with increased incidences of cardiovascular events and long-term risk of heart disease (Pope *et al.*, 2004). Prominent mechanisms of particle-induced cardiovascular disease include alterations in the autonomic nervous system resulting in cardiac arrhythmia, chronic systemic oxidative stress, and inflammation leading to atherosclerotic plaque formation, endothelial dysfunction, and APR-induced thrombosis (Brook, 2008). Here, we propose that NP-induced APR triggers changes in lipid transport and metabolism, thus activating the atherogenic HMG-CoA reductase pathway

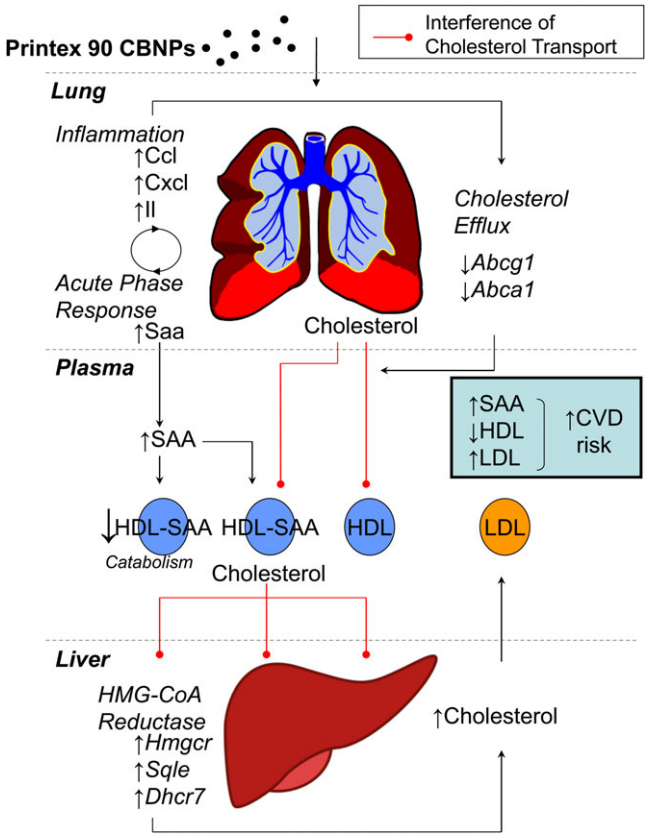

FIG. 2. Suggested mechanisms by which NPs may induce molecular signaling cascades leading to upregulation of the HMG-CoA reductase pathway in the liver of exposed C57BL/6 mice. We demonstrate that inflammation is induced by pulmonary deposition of nanomaterials, resulting in activation of APR. Secretion of APR reactants such as SAA into plasma is suggested to induce structural changes of HDL that may increase its catabolism and inhibit its capacity to associate with cholesterol, thus potentially inhibiting reverse cholesterol transport. Inflammation may also downregulate cholesterol efflux genes in lung (for example, *Abcg1* and *Abca1*), thus inhibiting cholesterol from reaching HDL. Such molecular changes inhibiting transport of excess cholesterol to liver for secretion into bile may lead to activation of the sterol-sensitive HMG-CoA reductase pathway in liver, leading to increased terpenoid and cholesterol synthesis. Increased SAA and LDL and decreased HDL are associated with cardiovascular disease risk.

(Fig. 2). The implication of the HMG-CoA reductase pathway in cardiovascular disease extends beyond excess cholesterol synthesis to endothelial nitric oxide expression and activation-mediated endothelial dysfunction (Rikitake and Liao, 2005), systemic oxidative stress–induced oxidation of LDL and activation of macrophages (Ilker-Yilmaz *et al.*, 2003), and release of proinflammatory factors that participate in leukocyte adhesion and progression of atherosclerotic lesions (Yoshida, 2003). In parallel, it has been suggested that HMG-CoA reductase inhibitors (i.e., statins) may be effective in preventing ambient particulate matter–induced coronary artery disease in individuals with elevated c-reactive protein levels, regardless of lipid profiles (Sandhu *et al.*, 2005). Further investigations are required to decipher the role of NPs in the disruption of cholesterol synthesis and metabolism and possible implications to metabolic and cardiovascular disease. At this time, it is unclear whether intratracheal instillations of NPs are expected to induce more substantive effects than exposure by inhalation. Although intratracheal instillation of Printex 90 CBNPs has been shown to cause more inflammation in terms of neutrophil influx in comparison to inhalation of the same dose (Jackson *et al.*, forthcoming; Jacobsen *et al.*, 2009), it has been shown that daily inhalation exposure to nano-titanium dioxide over 11 days and at doses well below the current occupational exposure limit resulted in pulmonary APR that persisted at least 5 days after the last exposure (Halappanavar *et al.*, 2011). This study is the first to simultaneously assess global lung and liver gene expression responses to CBNPs across various doses and extended to late time points to explore sustained molecular effects. The results provide important insights into NP-mediated systemic changes in APR, inflammation, and cholesterol homeostasis. The data indicate the power of a global systems biology approach to identify perturbed processes and identify candidate biological pathways supporting observed phenotypes.

SUPPLEMENTARY DATA

Supplementary data are available online at http://toxsci.oxfordjournals.org/.

FUNDING

Health Canada Genomics Research and Development Initiative, the Chemical Management Plan, and the Danish Working Environment fund (Nanokem, grant 20060068816 and NANOPLAST, grant 22-2007-03). Financial support for J.A.B. was through the Natural Sciences and Engineering Research Council of Canada.

ACKNOWLEDGMENTS

The authors would like to acknowledge Karen Leingartner for analysis of plasma and Shahram Eisa-Beygi for guidance with the Folch method. The authors also thank Michael Guldbrandsen, Lourdes Petersen, and Elzbieta Christiansen for their assistance. Furthermore, Azam Tayabali and Amal Malik are thanked for initial comments on the manuscript.

REFERENCES

Annema, W., Nijstad, N., Tolle, M., deBoer, J. F., Buijs, R. V. C., Heeringa, P., vanderGiet, M., and Tietge, J. F. (2010). Myeloperoxidase and serum amyloid A contribute to impaired in vivo reverse cholesterol transport during

the acute phase response but not group IIA secretory phospholipase A2. *J. Lipid Res.* **51,** 743–754.

Ballantyne, C. M., Hoogeveen, R. C., Bang, H., Coresh, J., Folsom, A. R., Heiss, G., and Sharrett, R. (2004). Lipoprotein-associated phospholipase A2, high-sensitivity c-reactive protein, and risk for incident coronary heart disease in middle-ages men and women in the atherosclerosis risk in communities (ARIC) study. *Circulation* **109,** 837–842.

Bourdon, J., Saber, A., Jacobsen, N., Jensen, K., Madsen, A., Wallin, H., Moller, P., Loft, S., Yauk, C., and Vogel, U. (2012). Carbon black nanoparticle instillation induces sustained inflammation and genotoxicity in mouse lung and liver. *Part. Fibre Toxicol.* **9,** 1–14.

Brook, R. (2008). Cardiovascular effects of air pollution. *Clin. Sci.* **115,** 175–187.

Dong, Z., Wu, T., Qin, W., An, C., Wang, Z., Zhang, M., Zhang, Y., Zhang, C., and An, F. (2011). Serum amyloid A directly accelerates the progression of atherosclerosis in apolipoprotein E-deficient mice. *Mol. Med.* **17,** 1357–1364.

Driscoll, K. E., Carter, J. M., Howard, B. W., Hassenbein, D. G., Pepelko, W., Baggs, R. B., and Oberdorster, G. (1996). Pulmonary inflammation, chemokine, and mutagenic responses in rats after subchronic inhalation of carbon black. *Toxicol. Appl. Pharmacol.* **136,** 372–380.

Feingold, K. R., and Grunfeld, C. (2010). The acute phase response inhibits reverse cholesterol transport. *J. Lipid Res.* **51,** 682–684.

Feingold, K. R., Hardardottir, I., Memon, R., Kral, E. J., Moser, A. H., Taylor, J. M., and Grunfeld, C. (1993). Effects of endotoxin on cholesterol biosynthesis and distribution in serum lipoproteins in Syrian hamsters. *J. Lipid Res.* **34,** 2147–2158.

Feingold, K. R., Pollock, A. S., Moser, A. H., Shigenaga, J. K., and Grunfeld, C. (1995). Discordant regulation of proteins of cholesterol metabolism during the acute phase response. *J. Lipid Res.* **36,** 1474–1482.

Gardiner, K., Van Tongeren, M., and Harrington, M. (2001). Respiratory health effects from exposure to carbon black: Results of the phase 2 and 3 cross sectional studies in the European carbon black manufacturing industry. *Occup. Environ. Med.* **58,** 496–503.

Halappanavar, S., Jackson, P., Williams, A., Jensen, K. A., Hougaard, K. S., Vogel, U., Yauk, C. L., and Wallin, H. (2011). Pulmonary responses to surface-coated nanotitanium dioxide particles includes induction of acute phase response genes, inflammatory cascades, and changes in microRNAs: A toxicogenomic study. *Environ. Mol. Mutagen.* **52,** 425–439.

Hellstrand, E., Lynch, I., Andersson, A., Drakenburg, T., Dahlback, B., Dawson, K. A., Linse, S., and Cedervall, T. (2009). Complete high-density lipoproteins in nanoparticle corona. *FEBS J.* **276,** 3372–3381.

Higgins, J. J. (2003). *An Introduction to Modern Nonparametric Statistics*. Brooks/Cole, Pacific Grove, CA.

Hollan, I., Scott, H., Saatvedt, K., Prayson, R., Mikkelsen, K., Nossent, H. C., Kvelstad, I. L., Liang, M. H., and Forre, O. T. (2007). Inflammatory rheumatic disease and smoking are predictors of aortic inflammation: A controlled study of biopsy specimens obtained at coronary artery surgery. *Arthritis Rheum.* **56,** 2072–2079.

Huang, D., Sherman, B., and Lempicki, R. (2009a). Bioinformatics enrichment tools: Paths toward the comprehensive functional analysis of large gene lists. *Nucleic Acids Res.* **37,** 1–13.

Huang, D., Sherman, B., and Lempicki, R. (2009b). Systematic and integrative analysis of large lists using DAVID bioinformatics resources. *Nat. Protoc.* **4,** 44–57.

Hubbs, A., Mercer, R., Benkovic, S., Harkema, J., Sriram, K., Schwegler-Berry, D., Goravanahally, M., Nurkiewicz, T., Castranova, V., and Sargent, L. (2011). Nanotoxicology—A pathologist's perspective. *Toxicol. Pathol.* **39,** 301–324.

International Agency for Research on Cancer (IARC). 2010. IARC monographs on the evaluation of carcinogenic risks to humans: Carbon black, titanium dioxide, and talc. Lyon, France, 452 pp. Available at: http://monographs.iarc.fr/ENG/Monographs/vol93/index.php. Accessed April 9, 2012.

Ilker-Yilmaz, M., Baykal, Y., Kilic, M., Sonmez, A., Bulucu, F., Aydin, A., Sayal, A., and Hakki-Kocar, I. (2003). Effects of statins on oxidative stress. *Biol. Trace Elem. Res.* **98,** 119–127.

Jackson, P., Hougaard, K., Vogel, U., Wu, D., Casavant, L., William, A., Wade, M., Yauk, C., Wallin, H., and Halappanavar, S. (2012). Exposure of pregnant mice to carbon black by intratracheal instillation: Toxicogenomic effects in dams and offspring. *Mutat. Res.* **745,** 73–83.

Jackson, P., Hougaard, K. S., Boisen, A. M. Z., Jacobsen, N. R., Jensen, K. A., Moller, P., Brunborg, G., Gutzkow, K. B., Andersen, O., Loft, S., *et al.* (Forthcoming). Pulmonary exposure to carbon black by inhalation or instillation in pregnant mice: Effects on liver DNA strand breaks in dams and offspring. *Nanotoxicology.*

Jacobsen, N., Saber, A., White, P., Pojana, G., Vogel, U., Loft, S., Gingerich, J., Soper, L., Douglas, G., and Wallin, H. (2007). Increased mutant frequency by carbon black, but not quartz, in the lacZ and cII transgenes of Muta^{TM}Mouse lung epithelial cells. *Environ. Mol. Mutagen.* **48,** 451–461.

Jacobsen, N. R., Moller, P., Vogel, K. A., Ladefoged, O., Loft, S., and Wallin, H. (2009). Lung Inflammation and genotoxicity following pulmonary exposure to nanoparticles in Apo -/- mice. *Part. Fibre Toxicol.* **6,** 1–7.

Jacobsen, N. R., Pojana, G., White, P., Moller, P., Cohn, C. A., Korsholm, K. S., Vogel, U., and Wallin, H. (2008). Genotoxicity, cytotoxicity, and reactive oxygen species induced by single-walled carbon nanotubes and C(60) fullrenes in the FE1-muta trade mark mouse lung epithelial cells. *Environ. Mol. Mutagen.* **49,** 476–487.

Kang, G. S., Gillespie, P. A., Gunnison, A., Moreira, A. L., Tchou-Wong, K.-M., and Chen, L.-C. (2011). Long-term inhalation exposure to nickel nanoparticles exacerbated atherosclerosis in a susceptible mouse model. *Environ. Health Perspect.* **119,** 176–181.

Liao, J. K. (2002). Isoprenoids as mediators of the biological effects of statins. *J. Clin. Investig.* **110,** 285–288.

Magari, S. R., Hausser, R., Schwartz, J., William, P. L., Smith, T. J., and Christiani, D. C. (2001). Association of heart rate variability with occupational and environmental exposure to particulate air pollution. *Circulation* **104,** 1–7.

McGillicuddy, F. C., de la Llera Moya, M., Hinkle, C. C., Joshi, M. R., Chiquoine, E. H., Billheimer, J. T., Rothblat, G. H., and Reilly, M. P. (2009). Inflammation impairs reverse cholesterol transport. *Circulation* **119,** 1135–1145.

Memon, R. A., Grunfeld, C., Moser, A. H., and Feingold, K. R. (1993). Tumor necrosis factor mediates the effects of endotoxin on cholesterol and triglyceride metabolism in mice. *Endocrinology* **132,** 2246–2253.

Moller, P., Jacobsen, N. R., Folkmann, J. K., Danielsen, P. H., Mikkelsen, L., Hemmingsen, J. G., Vesterdal, L. K., Forchhammer, L., Wallin, H., and Loft, S. (2010). Role of oxidative damage in toxicity of particulates. *Free Radic. Res.* **44,** 1–46.

Nikula, K. J., Snipes, M. B., Barr, E. B., Griffith, W. C., Henderson, R. F., and Mauderly, J. L. (1995). Comparative pulmonary toxicities and carcinogenicities of chronically inhaled diesel exhaust and carbon black in F344 rats. *Fundam. Appl. Toxicol.* **25,** 80–94.

Nurkiewicz, T. R., Porter, D. W., Barger, M., Millecchia, L., Rao, K. M., Marvar, P. J., Hubbs, A. F., Castranova, V., and Boegehold, M. A. (2006). Systemic microvascular dysfunction and inflammation after pulmonary particulate matter exposure. *Environ. Health Perspect.* **114,** 412–419.

Pfaffl, M. W., Horgan, G. W., and Dempfle, L. (2002). Relative expression software tool (REST©) for group-wise comparison and statistical analysis of relative expression results in real-time PCR. *Nucleic Acids Res.* **30,** e36.

Pope, C. A., III, Burnett, R. T., Thurston, G. D., Thun, M. J., Calle, E. E., Krewski, D., and Godleski, J. J. (2004). Cardiovascular mortality and long-

term exposure to particulate air pollution: Epidemiological evidence of general pathophysiological pathways of disease. *Circulation* **109,** 71–77.

R Development Core Team. (2010). *R: A Language and Environment for Statistical Computing*. R Foundation for Statistical Computing, Vienna, Austria.

Rikitake, Y., and Liao, J. K. (2005). Rho GTPases, statins, and nitric oxide. *Circ. Res.* **97,** 1232–1235.

Sadauskas, E., Jacobsen, N. R., Danscher, G., Stoltenberg, M., Vogel, U., Larsen, A., Kreyling, W., and Wallin, H. (2009). Biodistribution of gold nanoparticles in mouse lung following intratracheal instillation. *Chem. Cent. J.* **3,** 1–7.

Sandhu, R. S., Petroni, D. H., and George, W. J. (2005). Ambient particulate matter, c-reactive protein, and coronary artery disease. *Inhal. Toxicol.* **17,** 409–413.

Schins, R. P. F., and Knaapen, A. M. (2007). Genotoxicity of poorly soluble particles. *Inhal. Toxicol.* **19,** 189–198.

Vishwakarma, V., Samal, S., and Manoharan, N. (2010). Safety and risk associated with nanoparticles—A review. *J. Mineral and Mat. Char. Eng.* **9,** 455–459.

Yoshida, M. (2003). Potential roles of statins in inflammation and atherosclerosis. *J. Atheroscler. Thromb.* **10,** 140–144.